A new index used to characterise the extent of Antarctic marine coastal winds in climate projections

Archie Cable[1], Thomas Caton Harrison[2], Elizabeth Kent[1], Richard Cornes[1], and Thomas J. Bracegirdle[2]

[1]National Oceanography Centre, Southampton, UK
[2]British Antarctic Survey, Cambridge, UK

Correspondence: Archie Cable (acable@noc.ac.uk)

Abstract. Antarctic marine coastal near-surface winds play a key role in Southern Ocean circulation. Using the ERA5 re-analysis dataset, this paper develops directional wind constancy as a tool for identifying key features in these winds and their relationship with the mid-latitude westerly jet. In particular, the Antarctic coastal wind boundary (ACWB), defined as the minimum offshore directional constancy boundary, is shown to be a useful way to define the marine near-coastal region where the Antarctic topography plays an important role in influencing the wind direction. We show that, while the ACWB is linked to large-scale modes of atmospheric circulation through its close association with variability in the mid-latitude westerly jet, it also highlights key regions where topographically-influenced, meridional flows are dominant. These meridional flows are not identified in current regional climate indices. Future changes in the ACWB are examined using CMIP6 projections for a high emissions scenario. This indicates that by the end of this century the ACWB is projected to shift poleward by about 60 km, less than the 130 km shift in the mid-latitude westerly jet, indicating a reduction in the extent of the circumpolar trough.

1 Introduction

Near-surface winds over marine regions close to the Antarctic coast have far-reaching impacts on the global climate. These winds help explain the structure and variability of the Antarctic Slope Current, which is a key control on the transport of relatively warm circumpolar deep water towards ice shelves, driving basal melt (Thompson et al., 2018). Additionally, the volume and extent of sea ice is strongly influenced by Antarctica's coastal winds. In some regions, coastal winds help open coastal polynyas, which are important for the formation of Antarctic bottom water (AABW). AABW in turn forms the lower limb of the meridional overturning circulation, which transports heat and carbon across the globe (Schmidt et al., 2023). Finally, winds are important for Antarctic coastal ecosystems and for polar infrastructure and operations (Baring-Gould et al., 2005).

Near-coastal Antarctic winds are linked to the strong circumpolar westerlies at mid-latitudes: the 'westerly jet'. The region between the coastal easterlies and the westerly jet is often referred to as the circumpolar trough and exhibits strong wind variability due in part to cyclones spiraling poleward. Poleward of the circumpolar trough the winds are on average dominated by easterlies. However, the easterlies are not dominant at all longitudes, with strong meridional flow at some locations (Fig. 1). This is due to the Antarctic topography, which plays an important role in controlling the coastal winds. The arrows in Fig. 1
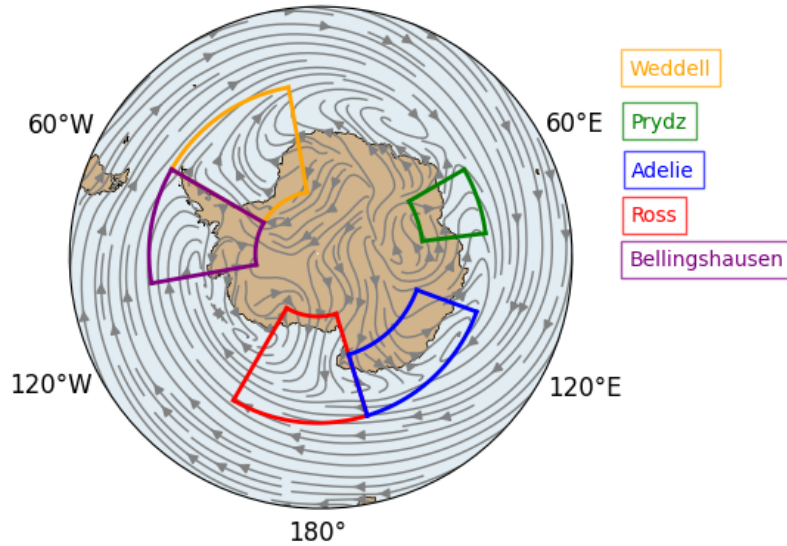
Figure 1. Winds around Antarctica. Grey arrows show the time-averaged winds from 1980–2023 using ERA5 monthly wind data. Highlighted regions are where extensive meridional winds prevail: Prydz Bay (60E–83E), Adélie Land (110E–163E), the Ross Sea (163E–150W), the Bellinghausen Sea (60W–100W) and the Weddell Sea (10W–60W).

25   represent the time-averaged wind fields from 1980–2023 using ERA5 wind data, illustrating their complex structure.

Highlighted in Fig. 1 are 5 key regions of extensive meridional winds, where the Antarctic topography is a leading driver. We refer to winds in these regions as "topographically-influenced", which encompasses a great variety of drivers (Turner et al., 2017; Goyal et al., 2021a; Orr et al., 2008; Lachlan-Cope et al., 2001). A primary example is katabatic winds, which are driven

30   by cold dense air in the surface boundary layer flowing down steep slopes. They prevail around much of the Antarctic coastline but are particularly extensive off Adélie Land (Parish et al., 1993; Davrinche et al., 2024) and Prydz Bay (Yu et al., 2024). Over the Ross Sea, the Transantarctic Mountains acts as a barrier to the zonal flow, creating local pressure gradients that drive the Ross Air Stream (RAS, Parish and Bromwich, 2002; Nigro and Cassano, 2014). Similarly, the Antarctic Peninsula has a strong influence on winds over the Weddell and Bellinghausen Seas (Parish, 1983; de Brito Neto et al., 2022; van Wessem et al., 2015).

35

Poleward shifting and strengthening of the westerly jet is a robust feature of projections using medium-high 21st century climate forcing scenarios (Goyal et al., 2021c). Although it is broadly found that coastal easterlies weaken as westerlies shift poleward (Bracegirdle et al., 2008; Neme et al., 2022), to date it has been a challenge to identify a simple index to characterise and quantify such changes. This guides the paper, which is structured around two related questions:

40

1. How is the extent of the Antarctic marine coastal winds projected to change in the future?

2. Can we robustly characterise the extent of these coastal winds across the entire Antarctic region?

The answer to the first question lies in the second. In order to study future projections of coastal winds and compare them to their mid-latitude counterparts, it is necessary to develop a robust way of characterising them on a circumpolar scale. In this paper we develop an approach based on directional wind constancy: a measure of how much the direction of the winds varies over a chosen period. We focus on the spatial pattern of monthly directional constancy, showing how features of the large- and local-scale winds are captured by this variable. We introduce the Antarctic coastal wind boundary (ACWB) as an index defining the latitude bounding the marine coastal winds region. We compare future projections of the ACWB and the latitude of the westerly jet to assess how the extent of the coastal winds region is projected to change in relation to the poleward-shifting westerlies.

The structure of the paper is as follows. In Sec. 2 and 3, we outline the data and methods used in our evaluation, before presenting some key features of directional constancy based on ERA5 in Sec. 4. In Sec. 4.1 and 4.2, we consider the spatial pattern of directional constancy around the Antarctic coastline and how it relates to variability in the mid-latitude winds, before examining the ACWB and its applications in Sec. 4.3 and 4.4. Finally, in Sec. 5, we consider how the ACWB is projected to change by the end of the century in relation to the mid-latitude westerly jet, using CMIP6 data.

2 Data

2.1 ERA5

We use wind data from the European Centre for Medium-Range Weather Forecasts' (ECMWF) 5th generation of reanalysis datasets, ERA5 (Hersbach et al., 2020, 2023). ERA5 is based on the ECMWF Integrated Forecasting System (IFS) using 4D-Var data assimilation. The surface wind output is an instantaneous value at a height of 10 m and is diagnostically derived using boundary layer theory from winds at the lowest model level (about 40 m height). Wind data is available hourly on a $0.25° \times 0.25°$ grid from 1940 to present; however, for this work, we will use monthly-averaged data from 1980 to 2023. This gives us 43 complete years of data in the satellite era, when ERA5 will be well constrained by observations. We use ERA5 as the primary dataset for this analysis as it exhibits the best performance when reproducing scatterometer data in the Antarctic coastal region when compared with other reanalysis datasets (Caton Harrison et al., 2022). A comparison with other reanalyses is given in Appendix A.

2.2 Climate models

We use a 27-member ensemble of atmosphere–ocean general circulation models that participated in the World Climate Research Programme's Coupled Model Intercomparison Project Phase 6 (CMIP6; Table S1). Models are included in the ensemble if the variables needed for our analysis are available (scalar wind speed and wind components at 10 m height) as well as a suitable land-sea mask. A list of chosen models is supplied in Table S1 of the Supplementary Material. For each model we analyse the high-emissions pathway SSP5-8.5 (Eyring et al., 2016). Future changes are evaluated for the periods 2020-2039, 2040-2059, 2060-2079 and 2080-2099 for each chosen model. Where multiple ensemble members are available we select only the first one. To enable inter-model comparison, every field is interpolated onto a common $1° \times 1°$ latitude–longitude grid spanning 90S–20S and 0–360E. Bilinear weights are computed with periodic boundaries in longitude, and models supplied on irregular native grids are mapped to a regular grid prior to interpolation. Land points are removed with each model's own land-sea mask.

3 Methods

3.1 Directional wind constancy calculation

Directional wind constancy (Singer, 1967) describes how much the wind direction varies over a chosen time period; here, we use monthly ERA5 wind data (Hersbach et al., 2020). It is defined as (Kodama et al., 1989)

$$c = \frac{\sqrt{u^2 + v^2}}{ws}, \tag{1}$$

where u and v are monthly-mean zonal and meridional wind components respectively, and ws is the monthly-mean wind speed. When c is smaller than one, the wind direction varies within the month; when $c = 1$, the winds are constant in direction. This parameter therefore uses monthly data to inform us of the directional variability of the winds at higher frequencies. Whilst the directional constancy doesn't provide details of the variability, such as the temporal autocorrelation time scales, or even the direction itself, it provides information that can be used to distinguish prevailing wind regimes, and even physical drivers in some cases.

3.2 Other circulation and wind indices

3.2.1 Antarctic Coastal Wind Boundary

As will be discussed in Sec. 4.1, the minimum offshore directional wind constancy is an important feature of the spatial structure. Thus, we define a new wind index - the *Antarctic coastal wind boundary* - as the latitude where the offshore directional constancy is at its lowest value in the region 60S-90S:

$$\text{ACWB}(t,\phi) = \theta(t,\phi)\big|_{\frac{\partial c}{\partial \theta}=0} \tag{2}$$

where θ, ϕ and t are latitude, longitude and time respectively. $\frac{\partial c}{\partial \theta} = 0$ indicates that we are taking the minimum value of the directional constancy as our latitude value at each time and longitude value. As will be discussed in Sec. 4.3, the ACWB provides a method for defining the boundary within which Antarctic coastal winds reside.

3.2.2 Minimum Zonal Wind Boundary

The dominant zonal flow close to the Antarctic coastline is easterly; however, towards the mid-latitudes, this switches to westerly. The minimum zonal wind boundary (MZWB) denotes where this switch occurs. It is defined as the latitude of minimum over-ocean (i.e. excluding land data but including sea-ice) magnitude of zonal wind between 60S and 90S and computed here using ERA5's 10 m wind data. In the literature, the MZWB is used to define the boundary of a study region, within which Antarctic coastal winds reside (Neme et al., 2022; Caton Harrison et al., 2022; Hazel and Stewart, 2019). Note that in the Ross and Weddell Seas, zonal winds are weak and a coastal buffer is typically required (e.g. 1000 m isobath, grid-box buffer) when defining the Antarctic coastal winds region using the MZWB.

3.2.3 The Southern Annular Mode index

Large-scale atmospheric circulation in the Southern Hemisphere is broadly zonally symmetric, and is often characterised with the Southern Annular Mode (SAM, Rogers and van Loon, 1982). The SAM plays an important role in the climate of the Southern Hemisphere as it provides a combined measure of the strength and latitude of the large-scale westerly jet in the mid-latitudes. For this paper, we use the SAM index as provided by the National Oceanic and Atmospheric Administration (NOAA), which uses 500 hPa geopotential height data from their Twentieth Century Reanalysis V2c Project (Compo et al., 2011). The SAM index is defined as the amplitude of the leading mode of variability in seasonal anomalies of 500 hPa geopotential height in the Southern Hemisphere (Mo, 2000).

3.2.4 The Jet Latitude Index

While the MZWB defines the transition zone where the time-mean zonal winds are weakest, the Jet Latitude Index (JLI) indicates the latitude at which the time-mean westerly winds are strongest. It is defined as the latitude of maximum time-mean zonal wind component between 10S and 75S at 850 hPa ($\sim$1500 m), following the definition by Bracegirdle et al. (2018). As they do, we compute it using ERA5 wind data.

Climate index	Description
ACWB	Latitude of minimum offshore directional constancy between 60S and 90S.
MZWB	Latitude of minimum zonal wind speed magnitude between 60S and 90S.
SAM	Amplitude of the leading mode of variability in seasonal anomalies of 500 hPa geopotential height in the Southern Hemisphere.
JLI	Latitude of maximum time-mean zonal wind component between 10S and 75S at 850 hPa.

Table 1. Summary of the key climate indices used in this paper, described in Sec. 3.2

3.3 Estimating large-scale winds

To quantify how spatial patterns of directional constancy are influenced by both local and large-scale factors, we compare directional constancy as calculated in Eq. 1 with a 'large-scale directional constancy'. Large-scale near-surface winds are derived by van den Broeke et al. (2002) and calculated from ERA5 reanalysis output in Caton Harrison et al. (2024). The large-scale term is defined as the linear extrapolation of the geostrophic wind profile at 300 hPa to 10 m above the surface under an idealised 'background' thermal wind balance. This provides an estimate of the role that large-scale pressure gradients alone play in the wind field, independent of surface-driven effects such as katabatic acceleration. The large-scale directional constancy is then calculated from these large-scale winds using Eq. 1. For more details, see Appendix B.

4 Structure of directional constancy

4.1 Spatial pattern of directional constancy

The 1980–2023 time-averaged directional wind constancy (Fig. 2a) shows high values along most of the Antarctic coastline, reducing to a band of low values further equatorward. We can compare this pattern with the large-scale directional constancy defined in Sec. 3.3. Fig. 2b shows the spatial differences between the actual and large-scale directional constancy, both averaged over time from 2010–2020 using ERA5 wind data. These patterns can tell us much about the different drivers of Antarctic coastal winds, leading us to establish the following broad structure:

1. Highly directionally constant winds are found over the Antarctic landmass. Here, a large radiative deficit occurs at near-surface levels, favouring high static stability and the establishment of katabatic flow over sloping terrain (Parish, 1988; Sanz Rodrigo et al., 2013; Bintanja et al., 2014; Vignon et al., 2019). Fig. 2b shows differences between the actual and large-scale directional constancy onshore, meaning a substantial portion of the actual directional constancy stems from the near-surface contribution. However, directional constancy remains high year-round despite weaker radiative cooling in summer, suggesting that large-scale adjustment of the flow to the topography of Antarctica still plays a key role in its directional constancy (Parish and Cassano, 2003). This finding is supported by the analysis of Davrinche et al. (2024) who note that large-scale flow over Adélie Land is often aligned with katabatic flow.
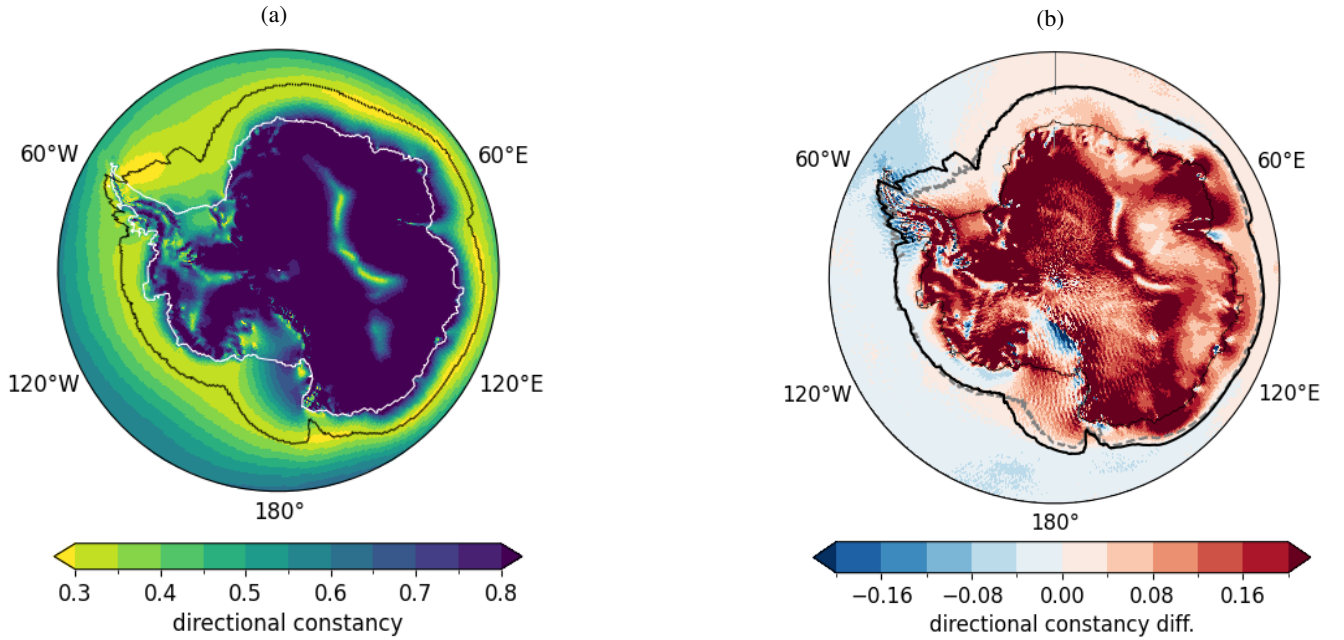
Figure 2. (a) The time-averaged directional constancy across the Antarctic region (60S–90S) from 1980–2023 using ERA5 wind data. Black contour indicates the time-averaged ACWB. (b) Also using ERA5 wind data, the difference between the actual and large-scale directional constancy, time-averaged from 2010–2020 (Caton Harrison et al., 2024). Black contour shows the time-averaged ACWB; grey, dashed line shows the ACWB for the calculated large-scale wind field.

2. High directional constancy also extends offshore and over ice shelves. Particularly high values ($c \sim 0.8$) occur in just a few regions, including around the western Ross Ice Shelf, Adélie Land and around western Prydz Bay. These are key sites of surface water mass transformation (Schmidt et al., 2023) and host frequent coastal polynyas during the winter months (Lin et al., 2024). Figure 2b shows that directional constancy in many offshore regions is higher than it would be under large-scale forcing alone. In the momentum budget analysis of Caton Harrison et al. (2024), these offshore regions of high directional constancy are where intense baroclinicity occurs due to diabatic cooling at low levels, which can occur even in the absence of sloping terrain (for example due to sea-ice, land-sea breezes and barrier effects). Some studies classify strong ice shelf winds as extensions of katabatic flow (Bromwich, 1989; Bromwich et al., 1993; King, 1993) although the slope of the terrain in these regions is near zero.

3. Further equatorward from the coast, directional constancy declines smoothly to a band of low values ($c \sim 0.3$). As will be discussed in more detail in Sec. 4.3, the location of the minimum directional constancy in Fig. 2a often aligns with the climatological minimum in the near-surface zonal winds: the MZWB as defined in Sec. 3.2.2. The exceptions correspond

to regions of significant meridional flow. Beyond the MZWB, the directional constancy increases further equatorward into the region dominated by westerly flow.

The black and grey lines in Fig. 2b show the ACWB, defined in Sec. 3.2.1, computed from the actual and large-scale directional constancy respectively. One can see that around most of the coastline, the locations are similar, meaning the large-scale behaviour dictates the position of this boundary. However, in the regions highlighted in Fig. 1, the differences become larger. Here, topographical flow extends further offshore and thus local influences have a strong impact on the position of the ACWB.

The main features of the spatial pattern of directional constancy (Fig. 2a) are present in each season (shown in Fig. S2). Additionally, seasonal, interannual and interdecadal variability are much smaller than the month-by-month variability seen in ERA5, indicating that the conditions in a given month are most important for controlling the position of the ACWB. Plots of the seasonal and interdecadal variability in the ACWB are given in Fig. S2 and S3 of the Supplementary Material.

4.2 Impacts of mid-latitude variability on the spatial pattern of directional constancy

To investigate whether large-scale synoptic modes of variability affect the spatial pattern of directional constancy, we perform a spectral decomposition using Empirical Orthogonal Functions (EOFs) on anomalies of the monthly directional constancy. We focus on the leading mode, which captures the large-scale structure of the variability in the directional constancy anomaly. Note that the leading mode only accounts for 25% of the variability across this large region, demonstrating the importance of the small-scale structure of these winds. We find that there is a high correlation of up to 0.71 between the principal component of the leading mode and the SAM index, suggesting that the leading variability in the directional constancy of Antarctic coastal winds is closely related to the the mid-latitude westerly jet. Note that this relationship is much weaker in higher-order modes; for the second principal component, the correlation drops to -0.22, and drops further for higher modes of variability.

Motivated by a strong correlation with the SAM, we perform a composite analysis, focusing on East Antarctica (0–160E). Consider the directional constancy composites based on the 10% most positive and negative leading principal component values, shown in Fig. 3. One can see that both Fig. 3a and 3b share the same structure as described above: high directional constancy over land (dark blue), reducing to a band of low directional constancy (bright yellow) offshore. The main difference between the figures is the strength and position of the band of lowest directional constancy. When the leading principal component is strongly positive (Fig. 3a), the band is close to and continuous around the coastline, although reducing in strength a little over Prydz Bay (60E–80E) and close to the Ross Sea (~150E). One can see this in the wind vectors (grey arrows). The highly directionally constant winds flow northward over the ice shelf and extend a little offshore. They begin to turn toward the west, but quickly vanish at the low band. At lower latitudes, they strengthen once again, now with a dominant westerly component. In contrast, the strongly negative principal component (Fig. 3b) shows the low band as weaker, less continuous and further offshore. While the onshore and katabatic winds don't change much, the south-easterly wind vectors extend further
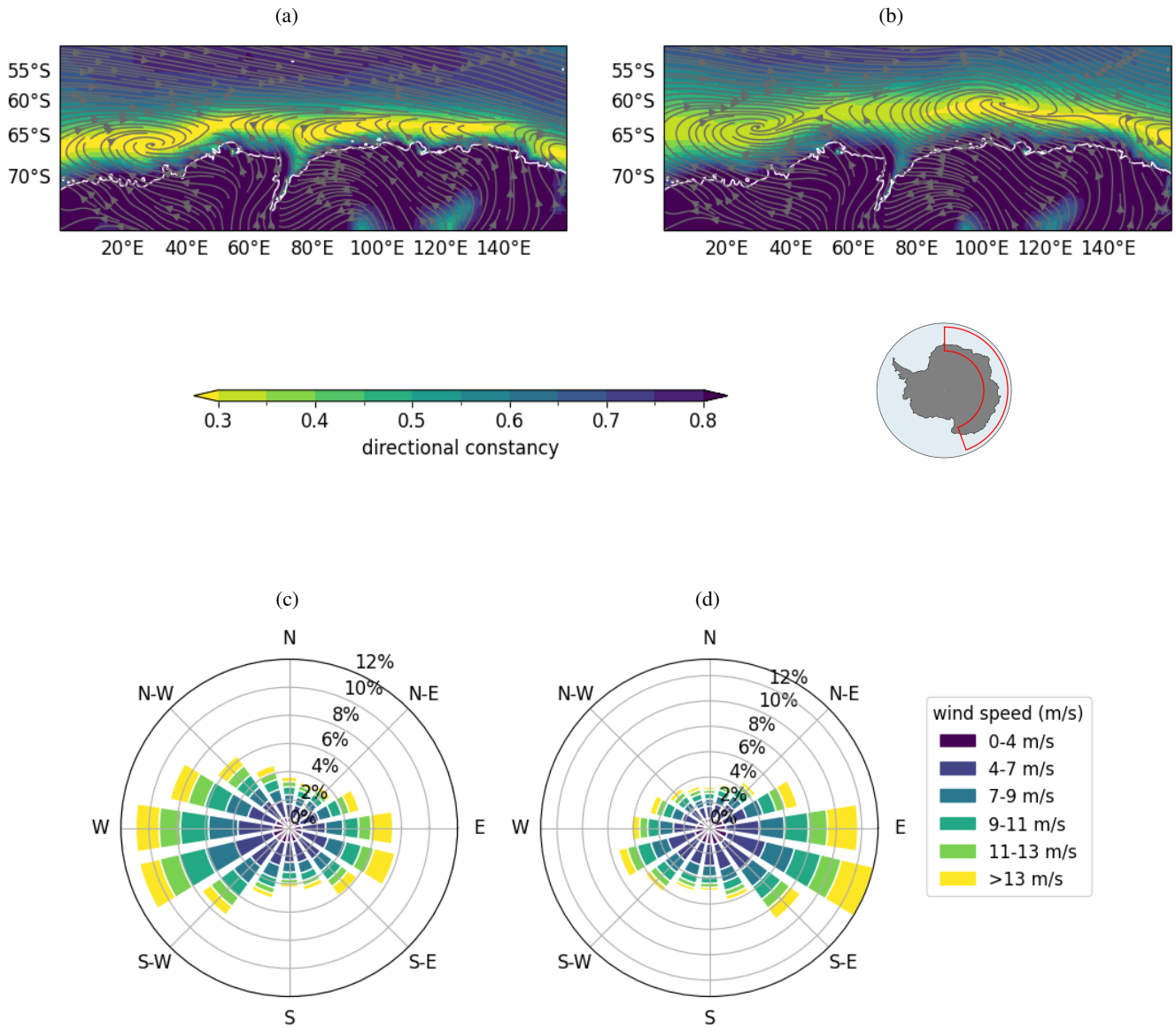
Figure 3. Directional constancy averaged over dates in the top (a) and bottom (b) 10% values in the leading principal component timeseries, using monthly ERA5 wind data in the East Antarctic region (red, boxed region on right map: 0-160E, 60S–90S). Grey arrows indicate the monthly winds averaged over the same dates. (c) & (d) are the wind rose plots, based on 6-hourly wind data over the ocean, associated with (a) and (b) respectively.

195 offshore before meeting the low directional constancy band and turning into westerlies. This difference is seen quite starkly in the wind rose diagrams (Fig. 3c and 3d), which show that the predominant offshore wind direction switches from westerlies

for high principal component values to south-east-easterlies for low values. Thus, we see that the leading mode of variability describes the position and strength of the large-scale zonal flow in relation to the Antarctic coastline.

200   ## 4.3   Antarctic coastal wind boundary

(a)   (b)
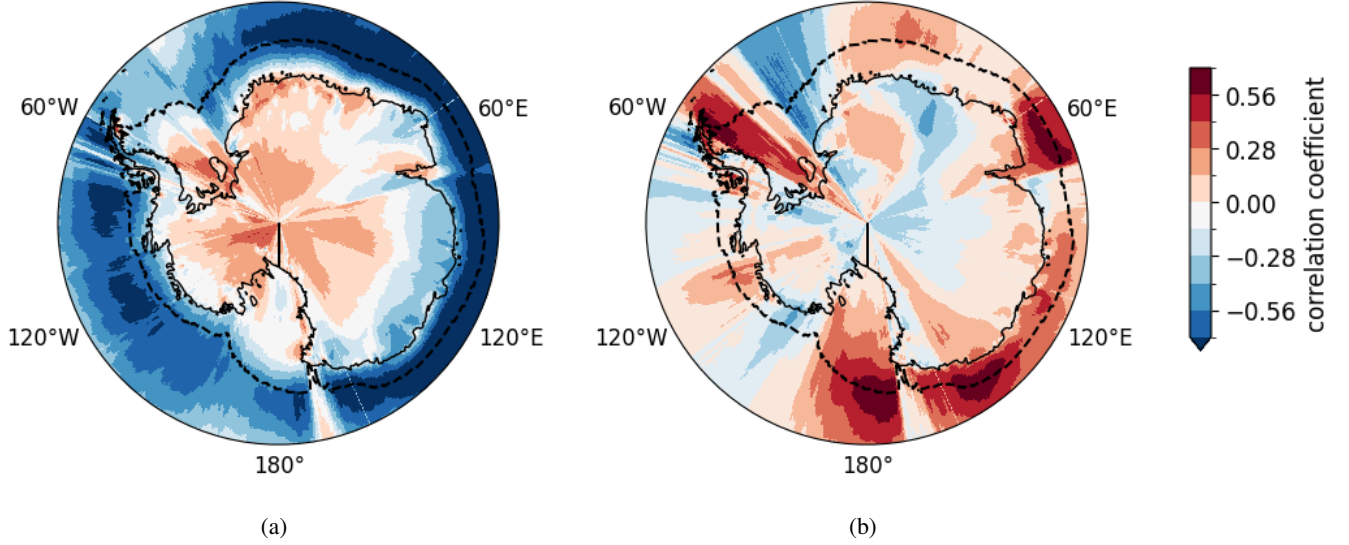
Figure 4. The correlation over time between the ACWB and the (a) zonal and (b) meridional component of 10 m ERA5 wind data from 1980–2023. Black dashed line indicates the time-averaged ACWB, again from 1980–2023. Jagged pattern occurs due to correlation between the ACWB and winds at a given longitude slice.

The ACWB, defined in Eq. (2), is a simple index that can be extracted from the directional constancy data and captures many of the key features in Antarctic coastal winds. To understand the extent to which the different wind components affect the ACWB, we consider their correlation over time, as shown in Fig. 4. Over the ocean, we see in Fig. 4a that the anti-correlation between the zonal wind and ACWB is strong (<-0.5) around most of the Antarctic coastline. This is particularly

205   strong on the eastern coastline, where the zonal flow is largely unimpeded by the topography. This tells us that, when the westerlies are stronger, the ACWB moves polewards, shrinking the region enclosed. In contrast, the correlation between the ACWB and meridional component is generally low; however, there are key hotspots, as shown by the red patches in Fig. 4b, where the correlation becomes higher (>0.5). This indicates that, when the meridional winds in these regions are strong, the ACWB moves further offshore. Note that these are the same regions where the large-scale directional constancy has less impact (Fig.

210   2b).

We can understand how the ACWB is related to the zonal wind component by comparing it with the MZWB, which defines the boundary between zonal easterlies and westerlies, as in Fig. 5. One can see by comparing the black and red lines in Fig. 5a that the two boundaries coincide around much of the Antarctic region. This is made clearer in Fig. 5b, where the fractional difference between the boundaries (red, upper line) is close to 0 at most longitudes. However, there are certain regions where the ACWB sits equatorwards of the MZWB; namely over the Weddell Sea, Ross Sea and small features offshore from Adélie Land and Prydz Bay. These are the same regions where the ACWB's correlation with the meridional component peaks (Fig. 4b) which is not captured by the MZWB, and the large-scale directional constancy has a lower impact (Fig. 2b) due to local topographic effects that extend off the coast. Here, the time-averaged zonal winds tend to be weak and thus the MZWB is less spatial coherent than the ACWB. Therefore, the ACWB provides a more comprehensive definition for the Antarctic coastal wind region than the MZWB, which is commonly used in the literature, as it not only describes the location where the zonal flow moves from easterly close to the coast to westerly towards the mid-latitudes, but also highlights key locations where meridional, topographically-influenced flow off the slopes becomes significant. This avoids the problem of having to define a buffer in these regions, unlike the study region defined by the MZWB.

(a)

(b)
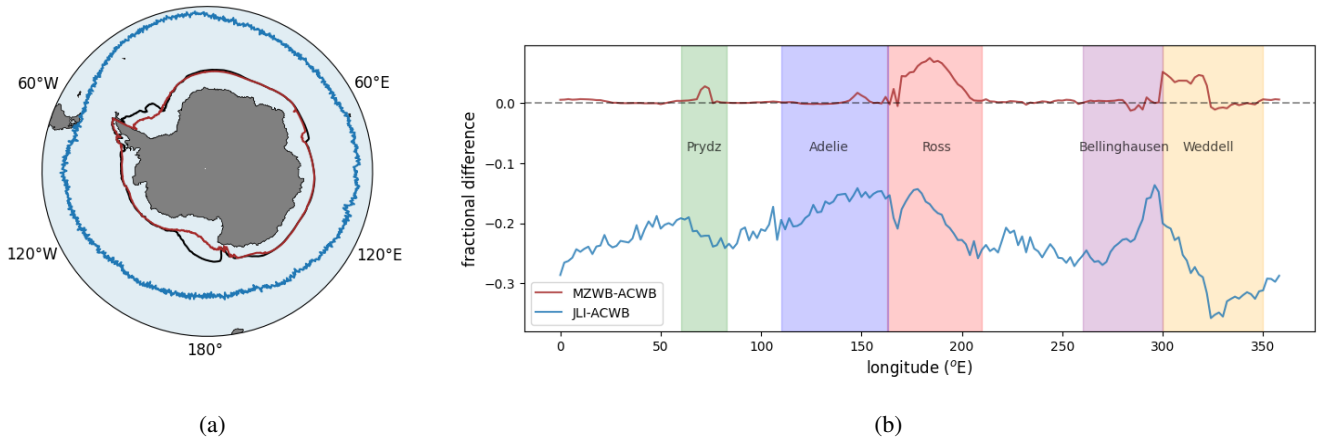
Figure 5. (a) A contour map of Antarctica with the time-averaged ACWB (red), MZWB (black) and JLI (blue) from ERA5 10 m wind data and (b) the difference between the MZWB and ACWB (black) and between the JLI and ACWB (blue), smoothed by 2° over longitude. Grey dashed line in (b) is zero fractional difference.

We also compare the ACWB and the JLI and find that the fractional difference (lower blue line in Fig. 5b) fluctuates with longitude. Additionally, the correlation over longitude between the ACWB and the JLI is 0.51: a non-negligible value. This highlights the relationship between the position of the mid-latitude westerly jet and the extent of Antarctic coastal winds. Note that the correlation between the MZWB and the JLI is slightly higher at 0.60, which is unsurprising as they are both defined

230 through zonal winds.

Finally, we will briefly mention the temporal correlation between the ACWB, SAM and JLI, using monthly wind data. All correlations mentioned below have p-values considered statistically significant with a 99% confidence level. Note that we have also compared the ACWB with other Scientific Committee on Antarctic Research (SCAR) Antarctic climate indicators, namely

235 the Jet Speed Index (Bracegirdle et al., 2018) and the Zonal Wave Number 3 (Raphael, 2004; Goyal et al., 2021b, 2022), but we find there to be very little correlation with the ACWB. However, the SAM and JLI indices have a reasonable degree of correlation with the ACWB - both 0.65 - which is similar to the correlation between the JLI and SAM (0.64). This again demonstrates the influence of the mid-latitude westerlies on the ACWB. We also consider the ACWB in two sectors: one covering the east (0–160E), the other the west (160E–0) Antarctic region. This definition includes the entire Ross Sea region in the

240 western side. We have seen already that the east coast is very closely related to the MZWB, whereas the west coast contains more topographical features, and a similar pattern manifests itself here. The correlation between the SAM and JLI indices and the eastern ACWB is higher - 0.69 and 0.67 respectively - but drops (0.51 and 0.55 respectively) when only the western coast is considered. This is because the western slopes contain two major geographic features - the Transantarctic Mountains and the Antarctic Peninsula - that interfere with the zonal flow. This again demonstrates that, while the mid-latitude winds have an

245 impact on their coastal counterparts, topographical influences cannot be neglected.

The spatial structure of directional constancy is broadly consistent year-round (Fig. S1) but the relationship between the ACWB and large-scale climate indices is stronger in austral summer than in winter. A robust assessment of seasonal climate drivers is beyond the scope of this paper, but this seasonality likely reflects the stronger topographic control of winds in winter.

250

4.4 Example: The Ross Sea

We have shown that the large-scale structure of the ACWB is closely related to the zonal flow around the continent except in some key regions. One such region is the Ross Sea, where the offshore winds are strongly influenced by local topography. The Transantarctic Mountains on the west provide a barrier to the easterly flow, and so winds flowing off the Ross Ice Shelf persist

255 further offshore on the western side of the Ross Sea, creating the Ross Ice Shelf air stream (RAS, Parish and Bromwich, 2002), before turning into westerlies around the ACWB. On the eastern coast exists a semi-permanent cyclone to the north west of Marie Byrd Land (north-eastern slopes), around 150W-160W. This Ross Cyclone is an important factor in driving the RAS (Parish et al., 2006).

260 We can identify these features in the directional constancy. Fig. 6a and 6b show directional constancy heatmaps, composited by the area enclosed by the ACWB in the Ross Sea in the 90th (largest area) and 10th (smallest area) percentile respectively. The main feature is the band of high directional constancy (shown in blue) near the western slopes, which begins over the Ross Ice Shelf and extends out over the Ross Sea, indicating the persistent southerly winds of the RAS. This is strengthened by
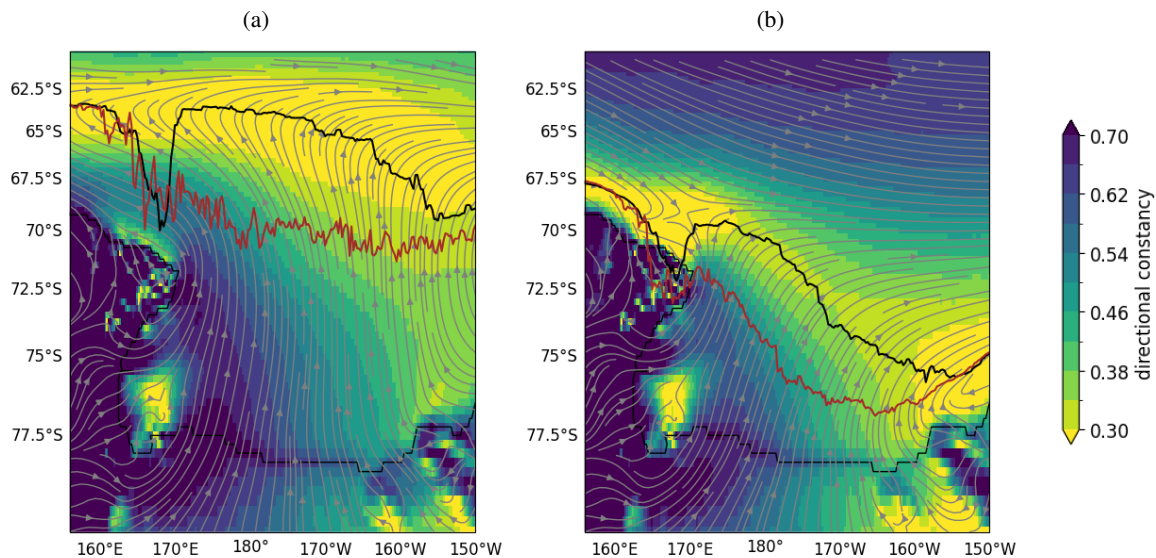
Figure 6. Directional constancy heat maps over dates where the area enclosed by the ACWB is, on average, in the (a) 90th and (b) 10th percentile in the Ross Sea, using ERA5 wind data. Black and red lines are the ACWB and MZWB respectively, averaged over the relevant dates. Grey arrows are monthly wind vectors, similarly averaged over the same dates.

winds flowing off the west slopes from the Transantarctic Mountains. One can see in Fig. 6a that, when the RAS is strongest

265   it extends further into the Ross Sea and offshore. The meridional flow is maintained until it turns to the east at the ACWB, breaking through the low directional constancy contour. Conversely, when the RAS is weakest (Fig. 6b), the blue band is confined to the western slopes and the wind speed drops to near-zero before turning to westerlies. This results in a band of low directional constancy, which is intersected by the ACWB. To the east of the RAS, the low and variable winds at the centre of the Ross Cyclone appear as an area of low directional constancy. When the meridional winds are strongest across the region,

270   this location tends to be further offshore and more distinct (Fig. 6a), compared to when the meridional winds are weakest, where it hugs the coastline (Fig. 6b).

Note also that there is an area of low directional constancy close to the coast in Terra Nova Bay (165E,77S). This region is prone to intense katabatic wind events, rather than consistent flow, meaning the winds there are highly variable (Guest, 2021).

275   This results in a spike of a higher latitude value in the ACWB. ERA5 picks this feature up particularly clearly due to its high resolution; other atmospheric reanalysis products don't to the same degree (see Appendix A for a comparison).

Consider now the ACWB and MZWB, which are plotted in Fig. 6 as the red and black, dashed lines respectively. In this region, they are quite different: the ACWB is much smoother and sits around the position where the dominant direction changes

from southerly to westerly. Conversely, the MZWB is noisy and cuts across the RAS (Fig. 6a). It is clear that the weak zonal
component of the near-coastal winds is sensitive to noise in this region, especially when the RAS is strong, whereas the
meridional contribution to the ACWB means it retains continuity. Additionally, the MZWB does not capture important aspects
of the regional wind structure, again particularly when the RAS is strong, such as the flow turning west around 67S, whereas
the ACWB does. This example highlights how the ACWB is an improved parameter for identifying the northern extent of
Antarctic coastal winds.

5 Future projections

(a)   (b)
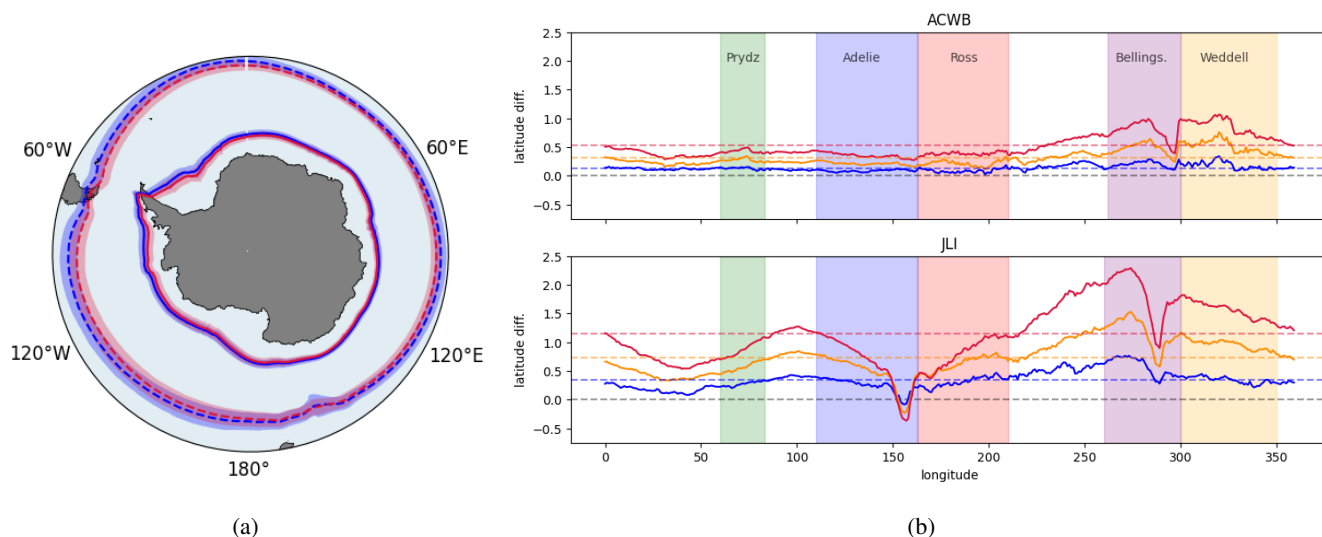
Figure 7. (a) The time-averaged JLI (dashed) and ACWB (solid) for the multi-model means of CMIP6, 2020–2039 (blue) and CMIP6,
2080–2099 (red). The shaded regions are the ±1 standard deviation of the CMIP6 models. (b) The difference between the 2020–2039 and
2080–2099 (red, upper), 2060–2079 (orange, middle), 2040–2059 (blue, lower) models for the JLI (bottom plot) and ACWB (top plot). The
dashed, coloured lines are the mean difference over latitude, while the grey dashed line is zero.

We will finally consider how the ACWB and JLI are projected to change in the future, using CMIP6 models under a high
emissions (SSP5-8.5) scenario. We have found that, although there are some differences in the ACWB between ERA5 and
CMIP6, the spatial pattern is very similar (Fig. C1a). We compare this in more detail in Appendix C. We consider the highest
emission scenario to highlight the projected behaviour of the boundaries. The same behaviour is prevalent in lower emission
scenarios but to a lesser degree. This can be seen in Fig. S4 of the Supplementary Materials.

We will compare 3 twenty-year future time periods - 2040–2059, 2060–2079 and 2080–2099 - with a baseline, near-term
period of 2020–2039. Fig. 7a shows the ACWB (solid) and JLI (dashed) for the near-term, 2020–2039 period (blue) and the

farthest-future, 2080–2099 period (red). In both cases, the boundaries are projected to shift poleward under climate change. However, it is apparent that the JLI is expected to shift further than the ACWB, which is seen more clearly when we consider the difference between the near-term and far-future boundaries in Fig. 7b. Here, we show all three far-future periods: 2040–2059 (blue, lower), 2060–2079 (orange, middle) and 2080–2099 (red, upper). We see that in both the ACWB (top) and JLI (bottom), there is a progressive reduction in the area bounded as we move forward in time, suggesting a forced response rather than inter-annual or inter-decadal variability. However, the ACWB shrinks far less - on average by $0.5°$ (60 km) by the end of this century - than the JLI, which on average shrinks by $1.1°$ (130km). This shows that the region of Antarctic marine coastal winds is not projected to move poleward to the same degree as the mid-latitude westerly belt. Rather, a reduction is seen in the extent of the highly-variable winds of the circumpolar trough. Such a reduction could have implications for carbon and heat uptake (Russell et al., 2018) and atmospheric blocking (Patterson et al., 2019).

Note that there is a distinction in the changes between the eastern (0–160E) and western (160E–0) areas. The eastern portion is projected to shrink less in both cases: $0.4°$ (40 km) and $0.8°$ (90 km) on the east compared to $0.6°$ (70 km) and $1.4°$ (160 km) on the west, for the ACWB and JLI respectively. It is notable that, in the western region where the Antarctic and mid-latitude winds are found to be less related, the JLI is due to shrink by almost 90 km more than the ACWB, compared to only 50 km more on the east.

6 Conclusions

This paper assesses how characteristics of the Antarctic coastal wind region may change in the future and develops a new index to quantify this. It is based on directional wind constancy: a parameter that describes the directional variability of winds over a chosen time period. By combining zonal and meridional wind components, it helps to distinguish between two regions of broadly directionally constant flow: the mid-latitude westerly jet and the topographically-influenced Antarctic coastal winds. The latter have a strong easterly component driven by large-scale pressure gradients, but are also strongly influenced by Antarctic topography. We have shown that directional constancy is sensitive to both these drivers. The large-scale pattern is that of high directional constancy near the shore and low directional constancy further offshore, highlighting the location where the average zonal wind direction switches from easterly in the Antarctic region to westerly in the mid-latitudes. Highly directionally-constant winds in certain marine regions - namely the Weddell and Bellinghausen Seas, the Ross Sea, Adélie Land and Prydz Bay - disrupt the coastal easterlies and are a result of the influence of topography on both large-scale and mesoscale pressure patterns.

Given this circumpolar band-like structure, we define the Antarctic coastal wind boundary (ACWB) as the latitude of minimum offshore directional constancy. In general, it defines the boundary where the mid-latitude westerlies switch to coastal easterlies, except in the identified key regions where the meridional flow dominates. Here, it correlates strongly with the merid-

ional wind component. This better identifies the northern boundary of Antarctic coastal winds, compared to the minimum zonal wind boundary (MZWB) typically used in the literature, because it captures the full extent of these topographic flows. A clear example of this is in the Ross Sea, where the ACWB contours the Ross Ice Shelf air stream, whereas the MZWB cuts through it.

In order to evaluate the stability of the ACWB under climate change, we considered how it is related to well-known changes to mid-latitude climate indices, such as the Jet Latitude Index (JLI) and the Southern Annular Mode (SAM). We have seen that, while the large-scale structure of coastal winds is strongly influenced by mid-latitude drivers, topographical drivers cannot be ignored as they give rise to important local features. In particular, the ACWB is useful as a near-coastal climate index, which can be compared to equivalent mid-latitude indices like the JLI.

We put this into practice to study how the Antarctic coastal wind region is projected to change by the end of this century in comparison to the poleward-shifting westerly jet. We have computed the ACWB using CMIP6 climate models in a high emissions scenario, and compare it with future projections of the JLI. We find that, while the westerly jet is projected to shift southward by 130 km on average, the Antarctic region is more stable, only shrinking by 60 km. This suggests that, although the westerly jet is closely connected to the northern extent of Antarctic coastal winds, other regional factors may limit their southward contraction under climate change. This further suggests a reduction in the spatial extent of the highly variable winds of the circumpolar trough region. This work provides a platform for studying the structure and strength of the winds within the ACWB, and how they will change in the future.

Antarctic coastal winds are major drivers of Southern Ocean circulation and sea-ice variability. We have described an index that can be robustly calculated across model datasets, including future projections. This index can be used to relate the mid-latitude westerly jet directly to Antarctic coastal winds. Our analysis suggests that, although the two are closely related, they cannot be conflated. Understanding the relationship between mid-latitude and polar winds will be important for constraining future projections of the Antarctic climate.

Appendix A: Comparison of reanalysis datasets

For this paper, we have used the ERA5 wind data as there is evidence to suggest it does the best job at capturing Antarctic coastal winds when compared to other reanalysis products (Caton Harrison et al., 2022). However, it is still worth comparing some of our results with 3 additional reanalysis datasets - JRA3Q (JMA, 2023), JRA55 (JMA, 2013) and MERRA2 (GMAO, 2015). Fig. A1 shows the fractional differences between the directional constancy climatology of the 4 reanalyses.

Over the ocean, the agreement is generally good, with less than 0.05 absolute fractional difference in most locations, especially further offshore. However, near the coastline, the differences become more pronounced, particularly on the west side. MERRA2 predicts consistently higher directional constancy along the western coastline, particularly over the Ronne (in the
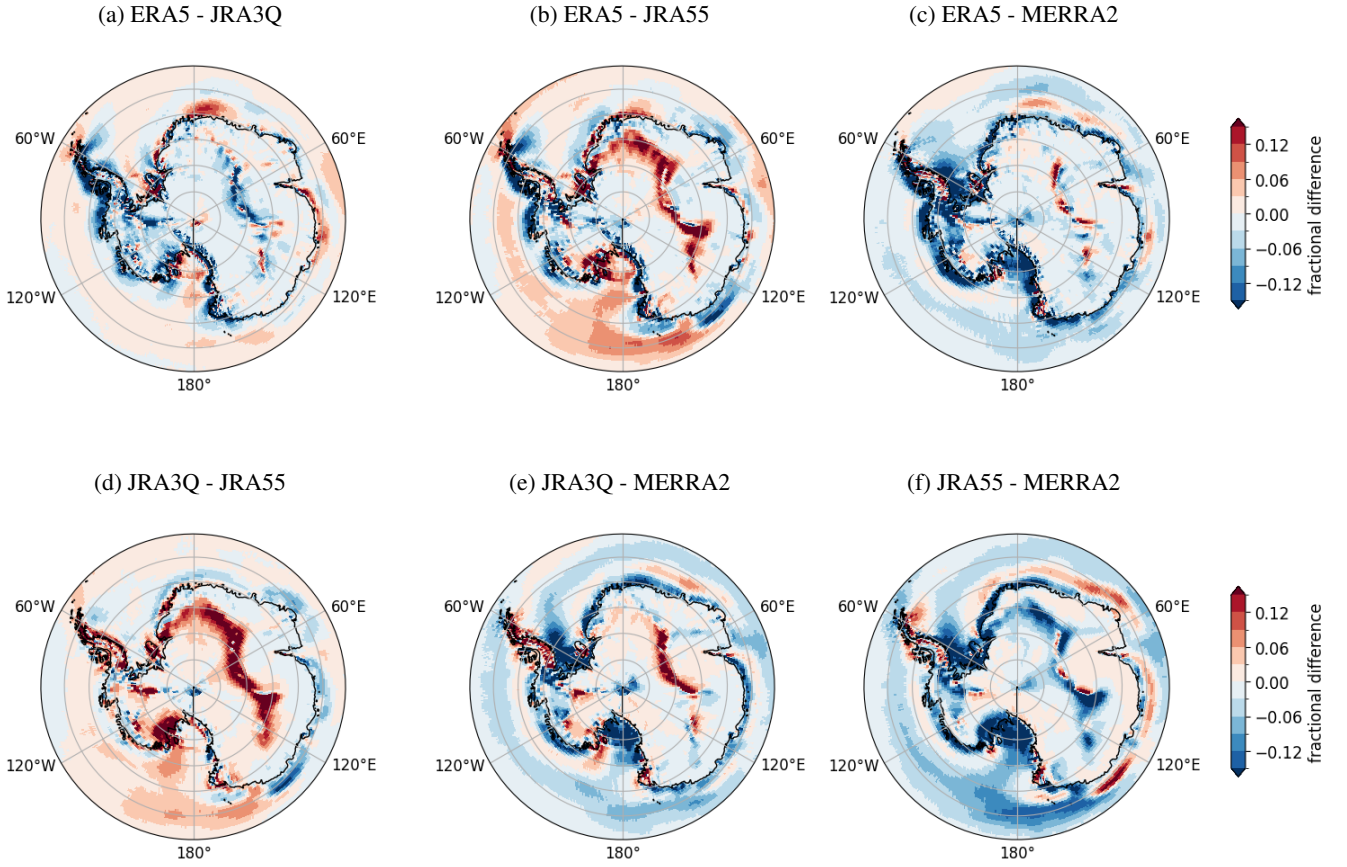
Figure A1. The fractional difference of the mean directional constancy, calculated from monthly wind data, between the 4 reanalysis products. Fractional difference calculated, for example, between ERA5 & JRA3Q as $\frac{2(\text{ERA5}-\text{JRA3Q})}{\text{ERA5}+\text{JRA3Q}}$.

Weddell Sea) and Ross Ice Shelves. These differences become more pronounced when comparing with the higher resolution ERA5 data. Indeed, the higher resolution data tends to predict a lower average directional constancy along the western coastline, particularly around the Antarctic Peninsula. It is likely because the higher resolution and improved representation of the orography picks up smaller-scale events that cause higher wind variability across a localised region.

365

We also compare the absolute fractional difference of the time-averaged ACWB between the reanalyses, as in Fig. A2. On average, the agreement tends to be quite good, with an absolute fractional difference of up to 0.007 at most longitudes. However, it is clear that MERRA2 differs the most from the other three reanalyses, as shown by the solid lines. This matches the behaviour shown in Fig. A1. Again, it appears that the lower resolution data fails to pick up localised, near-coastal events,
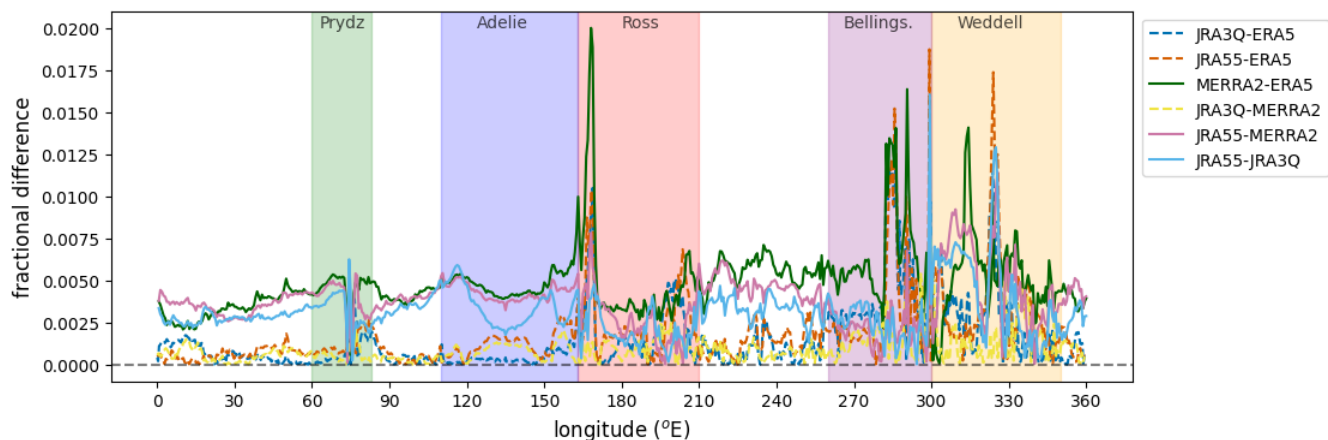
Figure A2. The absolute fractional difference (defined as in Fig. A1) between reanalysis datasets (coloured lines) for the time-averaged ACWB. Grey, dashed line indicates zero fractional difference.

370   which affects the ACWB.

In the Ross Sea, there is a sharp spike where the data disagree quite strongly. In particular, ERA5 predicts the ACWB to be at further south than the other reanalyses at around 165E. This is because it picks up an area of particularly low directional constancy in Terra Nova Bay (165E,77S), as seen in Fig. 6.

375

Finally, the ACWB across the Antarctic Peninsula (between the Weddell and Bellinghausen Seas) differs quite a lot across the reanalysis products. One can see from Fig. A1 that the high resolution products predict a lower directional constancy near the coastline, which is affecting the ACWB here. For example, there is a spike of difference between ERA5 and JRA55 on the west side of the Weddell Sea, where ERA5 predicts a region of low directional constancy at the tip of the Peninsula, a feature

380   that is not so prominent in JRA55.

Overall, one can see that the resolution of the reanalysis model contributes significantly to the location of the ACWB and to the structure of directional constancy very near the coastline. This supports conclusions drawn by Caton Harrison et al. (2022), who stated that ERA5 exhibits the best overall performance in regions where conditions favour katabatic forcing when

385   compared to scatterometry data. We conclude that the higher resolution of ERA5, compared to the other reanalyses, plays an important role in this improved behaviour.

Appendix B: Large-scale winds

The large-scale directional constancy is computed following Caton Harrison et al. (2024) and summarised here. First, the geostrophic horizontal wind at 300 hPa height, u_g and v_g, is calculated:

$$u_g = -\frac{g}{f}\frac{\partial \Phi}{\partial y}, \qquad v_g = \frac{g}{f}\frac{\partial \Phi}{\partial x}, \tag{B1}$$

where Φ is geopotential height, g gravity and f the Coriolis parameter. Next, vertical shear between 300 hPa and the surface pressure p_s is supplied by the thermal-wind relation using the background potential-temperature field θ_0:

$$\frac{\partial u_{\mathrm{lsc}}}{\partial \ln p} = \frac{R_d}{f}\frac{\partial \theta_0}{\partial y}, \qquad \frac{\partial v_{\mathrm{lsc}}}{\partial \ln p} = -\frac{R_d}{f}\frac{\partial \theta_0}{\partial x}, \tag{B2}$$

where $u_{lsc} = u_g$ and $v_{lsc} = v_g$ at 300 hPa, and R_d is the gas constant. Equation B2 is integrated to the surface and interpolated to 10 m height to obtain $u_{10,lsc}$ and $v_{10,lsc}$ (large-scale, near-surface winds). The background potential temperature θ_0 represents a smoothed profile which is equal to potential temperature except near the surface, where real potential temperature is sharply reduced due to radiative cooling (known as the temperature deficit). Background potential temperature is obtained by linearly extrapolating potential temperature from upper levels to the surface. Full details of the temperature-deficit formulation and its evaluation are given in Caton Harrison et al. (2024). Finally, $u_{10,lsc}$ and $v_{10,lsc}$ are substituted into Eq. 1 to obtain large-scale directional constancy.

Appendix C: Comparison of ERA5 reanalysis and climate models

We also compare ERA5 with the CMIP6 historical model from 1980–2010 (as described in Sec. 2.2), to test the performance of global climate models in capturing these boundaries and representing Antarctic marine coastal winds. We do this by comparing the ACWB and JLI.

Fig. C1a shows the two boundaries plotted around a map of Antarctica for ERA5 (blue) and the CMIP6 multi-model mean (orange). Consider first the JLI (dashed lines), which indicates the position of the strongest westerlies. The climate models consistently predict the JLI to be at lower latitudes than ERA5 at all longitudes. However, the correlation over longitude between the two is very high at 0.95. This suggests that the climate models are picking up the same spatial pattern in the westerlies as ERA5, but the whole position is slightly shifted away from the pole.

For the ACWB (solid lines), the climate models and ERA5 agree quite well along most of the coastline, particularly on the eastern side. Over the Amundsen and Bellinghausen Seas to the west of the Peninsula, the climate model predicts consistently lower latitudes than ERA5, with differences of order 1 standard deviation from the multi-model mean. The other exceptions

(a)   (b)
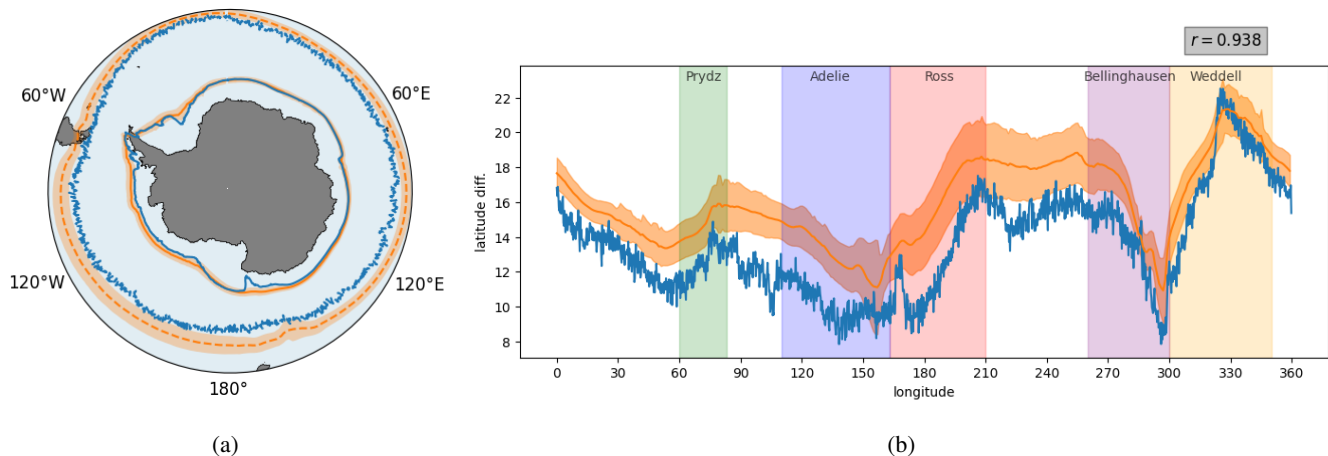
Figure C1. (a) The time-averaged JLI (dashed) and ACWB (solid) for ERA5 (blue) and CMIP6 historical multi-model mean (orange) from 1980–2010, and (b) the difference between the JLI and ACWB in both estimates. The shaded orange region is the ± 1 standard deviation of the CMIP6 models. The number in the grey box is the correlation over longitude between the two lines in (b).

are a small area around the Weddell Sea and to the west of the Ross Sea. It is probable that, in both cases, the higher resolution of ERA5 (0.25° as opposed to 1° for CMIP6) gives rise to features at the coastline that cause the ACWB to dip closer to the coast. Note also that we see a slight dip in the JLI at around 170E in CMIP6, which is caused by the split jet at that location (Chiang et al., 2018). Similar to the JLI, the correlation over longitude between the ACWB in climate models and ERA5 is extremely high at 0.94. This is encouraging as it suggests that the climate models are computing the same spatial pattern in the Antarctic coastal winds - both large-scale and topographically-influenced - as in ERA5, at least in the recreation of these boundaries.

For the projections, we will also compare the change in the JLI against those in the ACWB. Fig. C1b shows the difference between the JLI and ACWB for ERA5 (blue) and the historical CMIP6 multi-model mean (orange). One can see that the latitudinal difference between the ACWB and JLI is, on average, slightly larger in CMIP than ERA5. However, importantly, the correlation between these two lines is very high - 0.94 - and so, while ERA5 and CMIP6 disagree on the precise difference, they agree on the general behaviour, which is most important for our purposes. Thus, we can be confident that we will be capturing the correct variability in these boundaries using CMIP6, even if the precise latitudes are slightly different.

Supplement. The supplement related to this article can be found online at https://doi.org/10.5194/wcd-0-1-2025-supplement

Author contributions. AC with EK developed the initial concept for the analysis with further development from TCH, RC and TB. AC
435 developed the ACWB index and analysed the reanalyses. TCH analysed the climate models and made the large-scale directional constancy
calculations. All authors contributed to the revision of the initial paper draft by AC, and all authors have read and approved the submitted
version.

Competing interests. The contact author has declared that none of the authors have any competing interests

Data availability. ERA5 was downloaded from the Climate Data Store at https://cds.climate.copernicus.eu/datasets (Hersbach et al., 2023).
440 MERRA-2 was downloaded from the Goddard Earth Sciences Data & Information Services Center at https://disc.gsfc.nasa.gov/datasets?project=MERRA-
2 (GMAO, 2015). JRA-55 and JRA-3Q were both downloaded from the National Science Foundation (NSF) National Center for Environ-
mental Research (NCAR) Research Data Archive at https://rda.ucar.edu/lookfordata/ (JMA, 2013, 2023). CMIP6 model data was accessed
from the Earth Systems Grid Federation (ESGF) website at https://esgf-node.llnl.gov/search/cmip6/

Acknowledgements. AC, EK, TB and TCH were funded by NERC grant "Improved projections of winds at the crossroads between Antarctica
445 and the Southern Ocean" (NE/V000969/1 at NOC and NE/V000691/1 at BAS). RC received support from the NOC National Capability
Program AtlantiS (NE/Y005589/1). We are grateful to the European Centre for Medium-range Weather Forecasts (ECMWF), the NASA
Global Modeling and Assimilation Office (GMAO) and the Japan Meteorological Agency (JMA) for making ERA5, MERRA-2 and JRA-55
& JRA-3Q respectively. We acknowledge the World Climate Research Programme, which, through its Working Group on Coupled Modelling,
coordinated and promoted CMIP6. We thank the climate modeling groups for producing and making available their model output, the Earth
450 System Grid Federation (ESGF) for archiving the data and providing access, and the multiple funding agencies who support CMIP6 and
ESGF.

References

Amante, C. and Eakins, B.: ETOPO1 1 Arc-Minute Global Relief Model: Procedures, Data Sources and Analysis, NOAA Technical Memorandum NESDIS NGDC-24, NOAA National Geophysical Data Center, https://doi.org/10.7289/V5C8276M, accessed 20th February 2016, 2009.

Baring-Gould, I., Robichaud, R., and McLain, K.: Analysis of the Use of Wind Energy to Supplement the Power Needs at McMurdo Station and Amundsen-Scott South Pole Station, Antarctica, Tech. rep., National Renewable Energy Lab. (NREL), Golden, CO (United States), https://doi.org/10.2172/15016224, 2005.

Bintanja, R., Severijns, C., Haarsma, R., and Hazeleger, W.: The future of Antarctica's surface winds simulated by a high-resolution global climate model: 1. Model description and validation, J. Geophys. Res. - Atmos., 119, 7136–7159, https://doi.org/https://doi.org/10.1002/2013JD020847, 2014.

Bracegirdle, T. J., Connolley, W. M., and Turner, J.: Antarctic climate change over the twenty first century, J. Geophys. Res. - Atmos., 113, https://doi.org/https://doi.org/10.1029/2007JD008933, 2008.

Bracegirdle, T. J., Hyder, P., and Holmes, C. R.: CMIP5 diversity in southern westerly jet projections related to historical sea ice area: Strong link to strengthening and weak link to shift, J. Clim., 31, 195–211, https://doi.org/https://doi:10.1175/jcli-d-17-0320.1, 2018.

Bromwich, D. H.: Satellite Analyses of Antarctic Katabatic Wind Behavior, B. Am. Meteorol. Soc., 70, 738 – 749, https://doi.org/10.1175/1520-0477(1989)070<0738:SAOAKW>2.0.CO;2, 1989.

Bromwich, D. H., Carrasco, J. F., Liu, Z., and Tzeng, R.-Y.: Hemispheric atmospheric variations and oceanographic impacts associated with katabatic surges across the Ross ice shelf, Antarctica, J. of Geophys. Res. - Atmos., 98, 13 045–13 062, https://doi.org/https://doi.org/10.1029/93JD00562, 1993.

Caton Harrison, T., Biri, S., Bracegirdle, T. J., King, J. C., Kent, E. C., Vignon, E., and Turner, J.: Reanalysis representation of low-level winds in the Antarctic near-coastal region, Weather Clim. Dynam., 3, 1415–1437, https://doi.org/10.5194/wcd-3-1415-2022, 2022.

Caton Harrison, T., King, J. C., Bracegirdle, T. J., and Lu, H.: Dynamics of extreme wind events in the marine and terrestrial sectors of coastal Antarctica, Q. J. Roy. Meteor. Soc., 150, 2646–2666, https://doi.org/10.1002/qj.4727, 2024.

Chiang, J. C. H., Tokos, K. S., Lee, S.-Y., and Matsumoto, K.: Contrasting Impacts of the South Pacific Split Jet and the Southern Annular Mode Modulation on Southern Ocean Circulation and Biogeochemistry, Paleoceanogr. Paleoclimatol., 33, 2–20, https://doi.org/https://doi.org/10.1002/2017PA003229, 2018.

Compo, G. P., Whitaker, J. S., Sardeshmukh, P. D., Matsui, N., Allan, R. J., Yin, X., Gleason, B. E., Vose, R. S., Rutledge, G., Bessemoulin, P., Brönnimann, S., Brunet, M., Crouthamel, R. I., Grant, A. N., Groisman, P. Y., Jones, P. D., Kruk, M. C., Kruger, A. C., Marshall, G. J., Maugeri, M., Mok, H. Y., Nordli, O., Ross, T. F., Trigo, R. M., Wang, X. L., Woodruff, S. D., and Worley, S. J.: The Twentieth Century Reanalysis Project, Q. J. Roy. Meteor. Soc., 137, 1–28, https://doi.org/https://doi.org/10.1002/qj.776, 2011.

Davrinche, C., Orsi, A., Agosta, C., Amory, C., and Kittel, C.: Understanding the drivers of near-surface winds in Adélie Land, East Antarctica, The Cryosphere, 18, 2239–2256, https://doi.org/10.5194/tc-18-2239-2024, 2024.

de Brito Neto, F. A., Mendes, D., and Spyrides, M. H. C.: Analysis of extreme wind events in the Weddell Sea region (Antarctica) at Belgrano II Station, J. S. Am. Earth Sci., 116, 103 804, https://doi.org/https://doi.org/10.1016/j.jsames.2022.103804, 2022.

Eyring, V., Bony, S., Meehl, G. A., Senior, C. A., Stevens, B., Stouffer, R. J., and Taylor, K. E.: Overview of the Coupled Model Intercomparison Project Phase 6 (CMIP6) experimental design and organization, Geoscientific Model Development, 9, 1937–1958, 2016.

GMAO: Global Modeling and Assimilation Office, inst3_3d_asm_Cp: MERRA-2 3D IAU State, Meteorology Instantaneous 3-hourly (p-coord, 0.625x0.5L42), version 5.12.4, Greenbelt, MD, USA: Goddard Space Flight Center Distributed Active Archive Center (GSFC DAAC), https://doi.org/10.5067/3Z173KIE2TPD, accessed 01/10/2024, 2015.

Goyal, R., Jucker, M., Sen Gupta, A., and England, M. H.: Generation of the Amundsen Sea Low by Antarctic Orography, Geophys. Res. Lett., 48, e2020GL091 487, https://doi.org/https://doi.org/10.1029/2020GL091487, 2021a.

Goyal, R., Jucker, M., Sen Gupta, A., Hendon, H. H., and England, M. H.: Zonal wave 3 pattern in the Southern Hemisphere generated by tropical convection, Nat. Geosci., 14, 732–738, https://doi.org/https://doi.org/10.1038/s41561-021-00811-3, 2021b.

Goyal, R., Sen Gupta, A., Jucker, M., and England, M. H.: Historical and Projected Changes in the Southern Hemisphere Surface Westerlies, Geophys. Res. Lett., 48, https://doi.org/https://doi.org/10.1029/2020GL090849, 2021c.

Goyal, R., Jucker, M., Gupta, A. S., and England, M. H.: A New Zonal Wave-3 Index for the Southern Hemisphere, J. Clim., 35, 5137 – 5149, https://doi.org/10.1175/JCLI-D-21-0927.1, 2022.

Guest, P. S.: Inside Katabatic Winds Over the Terra Nova Bay Polynya: 1. Atmospheric Jet and Surface Conditions, J. Geophys. Res - Atmos., 126, e2021JD034 902, https://doi.org/https://doi.org/10.1029/2021JD034902, 2021.

Hazel, J. E. and Stewart, A. L.: Are the Near-Antarctic Easterly Winds Weakening in Response to Enhancement of the Southern Annular Mode?, J. Clim., 32, 1895 – 1918, https://doi.org/10.1175/JCLI-D-18-0402.1, 2019.

Hersbach, H., Bell, B., Berrisford, P., Hirahara, S., Horányi, A., Muñoz-Sabater, J., Nicolas, J., Peubey, C., Radu, R., Schepers, D., Simmons, A., Soci, C., Abdalla, S., Abellan, X., Balsamo, G., Bechtold, P., Biavati, G., Bidlot, J., Bonavita, M., De Chiara, G., Dahlgren, P., Dee, D., Diamantakis, M., Dragani, R., Flemming, J., Forbes, R., Fuentes, M., Geer, A., Haimberger, L., Healy, S., Hogan, R. J., Hólm, E., Janisková, M., Keeley, S., Laloyaux, P., Lopez, P., Lupu, C., Radnoti, G., de Rosnay, P., Rozum, I., Vamborg, F., Villaume, S., and Thépaut, J.-N.: The ERA5 global reanalysis, Q. J. Roy. Meteor. Soc., 146, 1999–2049, https://doi.org/https://doi.org/10.1002/qj.3803, 2020.

Hersbach, H., Bell, B., Berrisford, P., Biavati, G., Horányi, A., Muñoz Sabater, J., Nicolas, J., Peubey, C., Radu, R., Rozum, I., Schepers, D., Simmons, A., Soci, C., Dee, D., and Thépaut, J.-N.: ERA5 monthly averaged data on pressure levels from 1940 to present, https://doi.org/10.24381/cds.6860a573, accessed on 17-07-2024, 2023.

JMA: Japan Meteorological Agency/Japan. Updated monthly. JRA-55: Japanese 55-year Reanalysis, Daily 3-Hourly and 6-Hourly Data. Research Data Archive at the National Center for Atmospheric Research, Computational and Information Systems Laboratory., https://doi.org/https://doi.org/10.5065/D6HH6H41, accessed 16/09/2024, 2013.

JMA: Japan Meteorological Agency. Updated monthly. Japanese Reanalysis for Three Quarters of a Century (JRA-3Q). Research Data Archive at the National Center for Atmospheric Research, Computational and Information Systems Laboratory., https://doi.org/https://doi.org/10.5065/AVTZ-1H78, accessed 13/09/2024, 2023.

King, J. C.: Control of near-surface winds over an Antarctic ice shelf, J. Geophys. Res. - Atmos., 98, 12 949–12 953, https://doi.org/https://doi.org/10.1029/92JD02425, 1993.

Kodama, Y., Wendler, G., and Ishikawa, N.: The Diurnal Variation of the Boundary Layer in Summer in Adelie Land, Eastern Antarctica, J. Appl. Meteorol., 28, 16–24, https://doi.org/10.1175/1520-0450(1989)028<0016:TDVOTB>2.0.CO;2, 1989.

Lachlan-Cope, T. A., Connolley, W. M., and Turner, J.: The role of the non-axisymmetric antarctic orography in forcing the observed pattern of variability of the Antarctic climate, Geophys. Res. Lett., 28, 4111–4114, https://doi.org/https://doi.org/10.1029/2001GL013465, 2001.

Lin, Y., Nakayama, Y., Liang, K., Huang, Y., Chen, D., and Yang, Q.: A dataset of the daily edge of each polynya in the Antarctic, Sci. Data, 11, https://doi.org/https://doi.org/10.1038/s41597-024-03848-2, 2024.

525   Mo, K. C.: Relationships between Low-Frequency Variability in the Southern Hemisphere and Sea Surface Temperature Anomalies, J. Clim., 13, 3599 – 3610, https://doi.org/10.1175/1520-0442(2000)013<3599:RBLFVI>2.0.CO;2, 2000.

Neme, J., England, M. H., and McC. Hogg, A.: Projected Changes of Surface Winds Over the Antarctic Continental Margin, Geophys. Res. Lett., 49, e2022GL098 820, https://doi.org/10.1029/2022GL098820, 2022.

Nigro, M. A. and Cassano, J. J.: Identification of Surface Wind Patterns over the Ross Ice Shelf, Antarctica, Using Self-Organizing Maps,
530   Mon. Weather Rev., 142, 2361 – 2378, https://doi.org/10.1175/MWR-D-13-00382.1, 2014.

NOAA National Geophysical Data Center: ETOPO1 1 Arc-Minute Global Relief Model, https://www.ngdc.noaa.gov/mgg/global/global. html, NOAA National Centers for Environmental Information. Accessed 20th February 2016, 2009.

Orr, A., Marshall, G. J., Hunt, J. C. R., Sommeria, J., Wang, C.-G., van Lipzig, N. P. M., Cresswell, D., and King, J. C.: Characteristics of Summer Airflow over the Antarctic Peninsula in Response to Recent Strengthening of Westerly Circumpolar Winds, J. Atmos. Sci., 65,
535   1396 – 1413, https://doi.org/10.1175/2007JAS2498.1, 2008.

Parish, T. R.: The influence of the Antarctic Peninsula on the wind field over the western Weddell Sea, J. Geophys. Res. - Oceans, 88, 2684–2692, https://doi.org/https://doi.org/10.1029/JC088iC04p02684, 1983.

Parish, T. R.: Surface winds over the Antarctic continent: A review, Rev. Geophys., 26, 169–180, https://doi.org/https://doi.org/10.1029/RG026i001p00169, 1988.

540   Parish, T. R. and Bromwich, D. H.: Ross Island Meteorology Experiment (RIME), Detailed Science Plan, available from https://polarmet.osu.edu/RIME/pdf_docs/rim_sciplan_all_final.pdf, 2002.

Parish, T. R. and Cassano, J. J.: The Role of Katabatic Winds on the Antarctic Surface Wind Regime, Mon. Weather Rev., 131, 317 – 333, https://doi.org/10.1175/1520-0493(2003)131<0317:TROKWO>2.0.CO;2, 2003.

Parish, T. R., Pettré, P., and Wendler, G.: The influence of large-scale forcing on the katabatic wind regime at Adélie Land, Antarctica,
545   Meteorl. Atmos. Phys., 51, 165–176, https://doi.org/https://doi.org/10.1007/BF01030492, 1993.

Parish, T. R., Cassano, J. J., and Seefeldt, M. W.: Characteristics of the Ross Ice Shelf air stream as depicted in Antarctic Mesoscale Prediction System simulations, J. Geophys. Res. - Atmos, 111, https://doi.org/https://doi.org/10.1029/2005JD006185, 2006.

Patterson, M., Bracegirdle, T., and Woollings, T.: Southern Hemisphere Atmospheric Blocking in CMIP5 and Future Changes in the Australia-New Zealand Sector, Geophys. Res. Lett., 46, 9281–9290, https://doi.org/https://doi.org/10.1029/2019GL083264, 2019.

550   Raphael, M. N.: A zonal wave 3 index for the Southern Hemisphere, Geophys. Res. Lett., 31, https://doi.org/https://doi.org/10.1029/2004GL020365, 2004.

Rogers, J. C. and van Loon, H.: Spatial Variability of Sea Level Pressure and 500 mb Height Anomalies over the Southern Hemisphere, Mon. Weather Rev., 110, 1375 – 1392, https://doi.org/10.1175/1520-0493(1982)110<1375:SVOSLP>2.0.CO;2, 1982.

Russell, J. L., Kamenkovich, I., Bitz, C., Ferrari, R., Gille, S. T., Goodman, P. J., Hallberg, R., Johnson, K., Khazmutdinova, K.,
555   Marinov, I., Mazloff, M., Riser, S., Sarmiento, J. L., Speer, K., Talley, L. D., and Wanninkhof, R.: Metrics for the Evaluation of the Southern Ocean in Coupled Climate Models and Earth System Models, J. Geophys. Res. - Oceans, 123, 3120–3143, https://doi.org/https://doi.org/10.1002/2017JC013461, 2018.

Sanz Rodrigo, J., Buchlin, J., van Beeck, J., Lenaerts, J. T. M., and van den Broeke, M. R.: Evaluation of the Antarctic surface wind climate from ERA reanalyses and RACM02/ANT simulations based on automatic weather stations., Clim. Dyn., pp. 353–376,
560   https://doi.org/https://doi.org/10.1007/s00382-012-1396-y, 2013.

SCAR: Scientific Committee on Antarctic Research, https://scar.org/science/research-programmes/antclimnow/climate-indicators. Accessed in 26/08/2025.

Schmidt, C., Morrison, A. K., and England, M. H.: Wind– and Sea-Ice–Driven Interannual Variability of Antarctic Bottom Water Formation, J. Geophys. Res. - Oceans, 128, e2023JC019 774, https://doi.org/https://doi.org/10.1029/2023JC019774, 2023.

Singer, I. A.: Steadiness of the Wind, J. Appl. Meteorol., 6, 1033–1038, http://www.jstor.org/stable/26173250, 1967.

Thompson, A. F., Stewart, A. L., Spence, P., and Heywood, K. J.: The Antarctic Slope Current in a Changing Climate, Rev. Geophys., 56, 741–770, https://doi.org/https://doi.org/10.1029/2018RG000624, 2018.

Turner, J., Hosking, J. S., Bracegirdle, T. J., Phillips, T., and Marshall, G. J.: Variability and trends in the Southern Hemisphere high latitude, quasi-stationary planetary waves, Int. J. Climatol., 37, 2325–2336, https://doi.org/https://doi.org/10.1002/joc.4848, 2017.

van den Broeke, M. R., van Lipzig, N. P. M., and van Meijgaard, E.: Momentum Budget of the East Antarctic Atmospheric Boundary Layer: Results of a Regional Climate Model, J. Atmos. Sci., 59, 3117–3129, https://doi.org/10.1175/1520-0469(2002)059<3117:MBOTEA>2.0.CO;2, 2002.

van Wessem, J. M., Reijmer, C. H., van de Berg, W. J., van den Broeke, M. R., Cook, A. J., van Ulft, L. H., and van Meijgaard, E.: Temperature and Wind Climate of the Antarctic Peninsula as Simulated by a High-Resolution Regional Atmospheric Climate Model, J. Clim., 28, 7306 − 7326, https://doi.org/10.1175/JCLI-D-15-0060.1, 2015.

Vignon, E., Traullé, O., and Berne, A.: On the fine vertical structure of the low troposphere over the coastal margins of East Antarctica, Atmos. Chem. and Phys., 19, 4659–4683, https://doi.org/10.5194/acp-19-4659-2019, 2019.

Yu, L., Zhong, S., Xiao, E., Zhang, T., and Sun, B.: Near-surface wind variability in Prydz Bay and Amery Ice Shelf region, East Antarctica: A four-decade SOM analysis, Int. J. Climatol., 44, 5075–5089, https://doi.org/https://doi.org/10.1002/joc.8624, 2024.